Published by
NIGERIAN SOCIETY OF PHYSICAL SCIENCES
Available online @ https://journal.nsps.org.ng/index.php/jnsps

J. Nig. Soc. Phys. Sci. 8 (2026) 3086

Journal of the Nigerian Society of Physical Sciences

Effect of radial non-uniformity on mechanical response of functionally graded discs

Namarta Singh, Jatinder Kaur*

Department of Mathematics, Chandigarh University Gharuan, Mohali, Punjab-140413, India

Abstract

This study investigates the stress distribution in functionally graded material (FGM) discs composed of compressible and incompressible constituents, subjected to nonhomogeneity and external loading. Analytical results are presented for radial and tangential stresses as functions of the radii ratio r/b the gradation parameter m, and Poisson's ratio ν. However, the combined effect of compressibility and material gradation on the stress response of discs remains insufficiently explored, particularly in cases where both compressible ($\nu < 0.5$) and incompressible ($\nu \to 0.5$) material behaviors are considered under identical loading conditions. The methodology is designed to systematically evaluate how radial stress (σ_r) and tangential stress (σ_θ) evolve across the disc geometry in response to the combined influences of material gradation and volumetric compressibility. Figures are generated by MATLAB to provide comparative insights, separating compressible and incompressible cases, and highlighting the stress sensitivity to parameter variations. The focus of the investigation is twofold. First, the study seeks to establish the relationship between Poisson's ratio and stress magnitudes, particularly assessing whether compressible materials exhibit sharper stress gradients that could lead to structural instability. Second, the work examines the extent to which nonhomogeneity, represented by the parameter m, modifies these trends in both compressible and incompressible regimes. Furthermore, by delineating the contrasting behavior of compressible and incompressible FGMs, the study provides a decision-making basis for selecting appropriate material gradations in scenarios where crack initiation, fatigue resistance, or tensile failure are of concern. Thus, the present work sets out to systematically examine how compressibility and gradation interact to determine stress responses in FGM discs, with the ultimate objective of offering practical guidelines for the safe and efficient application of these advanced materials in engineering design.

DOI:10.46481/jnsps.2026.3086

Keywords: Non-homogeneous, FGM, Stresses, Strains, Thermoelasticity, Displacement

Article History :
Received: 11 August 2025
Received in revised form: 19 September 2025
Accepted for publication: 22 September 2025
Published: 31 October 2025

Communicated by: Pankaj Thakur

1. Introduction

Functionally graded materials (FGMs) were first introduced in 1984 by materials scientists in Japan's Sendai region as a way to create advanced thermal barrier materials. Unlike traditional materials, FGMs have properties like composition, microstructure, and porosity that change gradually, leading to smooth variations in characteristics such as mechanical strength and thermal conductivity according to Ref. [1]. This unique design makes FGMs ideal for high-performance applications, from super-refractory materials to cutting-edge functional components. Unlike uniform materials, FGMs are engineered com-

*Corresponding author Tel. No: +91-941-723-6509.
Email address: jksaini83@gmail.com (Jatinder Kaur)

posites with two or more phases, where properties like Young's modulus, Poisson's ratio, shear modulus, and density shift seamlessly in specific directions, offering superior performance [2].

Over the years, researchers have explored FGMs in various contexts. For instance, in 2015, ZW Wang and colleagues used an exponential function to study the mechanical properties of FGM vessels under internal pressure, applying the Euler-Cauchy formula to derive analytical solutions for thermo-mechanical stresses [3]. In 2016, Behravan and his team developed a semi-analytical 3D solution for transversely graded circular plates on non-uniform elastic foundations, with properties varying across the thickness[4]. A year later, Adineh *et al.* [5] examined the thermo-elastic behavior of multi-directional FGM rectangular plates under different boundary conditions, using the differential quadrature method to model temperature distribution.

In 2018, Habib *et al.* [6] investigated stress in an FGM cylinder with radially varying properties, using ANSYS software for finite element analysis. In 2019, Li *et al.* [7] studied a pressurized FGM arch in a thermal environment, noting how temperature-dependent properties affected displacement and Young's modulus. A 2020 study by Benslimane *et al.* [8] explored displacements and stresses in a thick-walled FGM cylinder, with elastic modulus and thermal conductivity varying radially while keeping Poisson's ratio constant; they solved Navier's differential equation for precise results.

In 2021, Arslan [9] examined the elastic limits of FGM pressure vessels under combined thermal and mechanical loads, using Reuss, Halpin-Tsai, and Voigt homogenization methods. In 2022, Benchallal *et al.* [10] analyzed stress and displacement in a rotating FGM thick-walled cylinder, with properties following a power-law distribution and solutions derived from Navier's second-order differential equation. In 2023, Lotfi *et al.* [11] tackled displacements, strains, and stresses in a porous FGM pressure vessel with variable thickness, applying higher-order shear deformation theory and a multi-layer method. Most recently, in 2024, Das *et al.* [12] studied how Poisson's ratio, internal pressure, temperature, and an inhomogeneity parameter influence stress and deformation in a rotating FGM pressure vessel, highlighting their role in controlling the thermoelastic behavior.

Gulial *et al.* [13] explores how steady-state creep and strain behave in an orthotropic rotating cylinder under external pressure, using Norton's law to analyze various steels and alloys across five types of anisotropy, finding that Types I and II anisotropic materials have lower effective stress than the isotropic Type III, while higher density boosts all stresses.

According to Singh *et al.* [14] how effective stress behaves in internally pressurized cylinders with varying density, using Norton's law to study a range of steels and alloys across five types of anisotropy, revealing that Type-I and Type-II anisotropic materials have lower effective stress than the isotropic Type-III, while higher density increases radial, circumferential, axial, and effective stresses.

Thakur *et al.* [15] investigates thermoelastoplastic stress deformation in a rotating cylinder crafted from orthotropic materials, specifically barite and copper, employing transition theory to establish the governing equations and derive analytical solutions. It examines the effects of temperature, angular speed, and stress distribution, revealing that circumferential stress is highest at the cylinder's inner surface for both materials, with thermal conditions causing angular speed to increase at the internal surface of barite but decrease in copper. Thakur *et al.* [15] explore the study on rotating disks made from natural rubber and polystyrene finds that the critical angular speed for yield initiation drops as radius ratio and axial load increase, with NR showing greater sensitivity due to thermal softening, while Polystyrene offers better mechanical stability, hoop stress, the primary driver of failure, decreases significantly in natural rubber at higher temperatures.

1.1. Limitations of existing literature

Research on rotating cylinders made of orthotropic materials has greatly improved our understanding of thermoelastoplastic stress and creep behavior. However, several important gaps still remain. Most studies tend to focus only on a few traditional materials like steel, barite, or copper, without exploring the possibilities offered by functionally graded materials, which could deliver far better performance through customized property variations. In addition, most investigations are confined to steady-state conditions or simplified loading cases, while practical applications often involve more complex situations such as dynamic, multi-axial, or impact loads critical in fields like aerospace and automotive engineering. Producing large components with precise, defect-free material gradients is not trivial, and sustainability concerns are rarely addressed, with little attention given to recyclable or eco-friendly alternatives that are becoming increasingly important in modern industry.

This paper address these limitations by examining the numerical analysis of mechanical properties in FGM discs, where material properties (Poisson's ratio, Elastic Modulus, Thermal Expansion, Temperature and Density of Material) vary radially using B.R Seth transition theory. This study investigates the influence of the non-homogeneity parameter on the radial and tangential stress ratios under applied load in composite materials. Graphical analysis will examines the stress distribution radially and circumferentially with variation of Poisson ratio and internal force applied at inner radius, of the FGM disc Using MATLAB, we simulate radial and circumferential stresses and strains to better understand how these advanced materials behave under different conditions.

2. Objectives of the study

The objective of study investigates the effect of variation on non homogeneity (m) and force applied at the external radii on the disc made of FGM material. Analyze the stress distribution in a functionally graded material disc composed of both compressible and incompressible components under a non-homogeneous external load. The obtained results are helpful in identifying the optimal material properties for structural applications and highlight the stress concentration risk in compressible material to prevent rupture.

2.1. Novelty of the study

This research presents a unique exploration of stress distribution in functionally graded material (FGM) discs, focusing on the combined effects of material compressibility, Poisson's ratio(ν), and gradation parameter (m) under non-homogeneous conditions and internal loading. Distinct from existing studies, it emphasizes the critical influence of (ν) on stresses, revealing that compressible materials (steel and copper) display increased stress intensities and sharper gradients along radially. The study's original contribution lies in its detailed comparison of compressible versus incompressible materials , demonstrating the latter's ability to achieve uniform stress profiles with minimal m impact. It further identifies specific regions prone to tensile failure in compressible materials, offering a fresh perspective on their cautious use in structural applications. By encouraging for incompressible-like FGMs to enhance stress distribution, this work provides new guidance for designing durable structural components, advancing material selection strategies.

3. Methodology

3.1. Problem statement and mathematical model

This study examines the response of non-homogeneous FGM disc made of compressible (steel, copper) and incompressible (rubber) subjected to applied force at the internal radius of the disc. Consider a thick-walled rotating disc with an inner radius a and outer radius b, rotating steadily about its axis at a constant angular velocity ω. The disc is assumed to be isotropic, and the problem is analyzed in cylindrical coordinates (r, θ, z), with displacement components defined as $u = r(1-\beta)$, $v = 0$, and $w = d \cdot z$, where β is a function of the radius and d is a constant according to Ref. [16]. The disc is modeled under plane stress conditions where $T_{zz} = 0$, which also implies that the plane strain condition is satisfied.

B. R. Seth's transition theory is used to elastic plastic transition in FGM material disc according to Ref. [17]. The evaluation of stresses, angular speed, and displacement components of a rotating isotropic disc by considering the variation in Young's modulus thermal expansion, Poisson's ratio, density, and thermal conductivity along the radial direction will be done using the following relation according to Ref. [18]:

$$E = E_0\left(\frac{r}{a}\right)^m \exp\left\{\gamma\left(\left(\frac{r}{a}\right)^s - 1\right)\right\}, \tag{1}$$

$$\alpha = \alpha_0\left(\frac{r}{a}\right)^m \exp\left\{\gamma\left(\left(\frac{r}{a}\right)^s - 1\right)\right\}, \tag{2}$$

$$\nu = \nu_0\left(\frac{r}{a}\right)^m \exp\left\{\gamma\left(\left(\frac{r}{a}\right)^s - 1\right)\right\}, \tag{3}$$

$$\rho = \rho_0\left(\frac{r}{a}\right)^m \exp\left\{\gamma\left(\left(\frac{r}{a}\right)^s - 1\right)\right\}, \tag{4}$$

$$k = k_0\left(\frac{r}{a}\right)^m \exp\left\{\gamma\left(\left(\frac{r}{a}\right)^s - 1\right)\right\}, \tag{5}$$

where $\gamma.m, s$ are constants and $E_0, \alpha_0, \nu_0, \rho_0$ *and* k_0 represents Young's modulus, thermal expansion, Poisson's ratio, density, and thermal conductivity. Further, the stresses will be observed numerically and graphically.

3.2. Boundary condition

The radial stress T_{rr} must satisfy the following conditions at the inner and outer radii of the disc:

(a) $T_{rr}(r = a) = 0$,

(b) $T_{rr}(r = b) = f_{out}$.

3.3. Governing equation

Seth [17] has previously defined the displacement components in cylindrical polar coordinates for the given system. For thermo-elastic isotropic materials, the stress-strain relationship is described by Parkus [19]:

$$T_{ij} = \lambda\delta_{ij}I_1 + 2\mu e_{ij} - \xi\Theta\delta_{ij}, (i, j = 1, 2, 3), \tag{6}$$

where $I_1 = e_{kk}$ is the first strain invariant, $\xi = \alpha(3\lambda + 2\mu)$, and Θ is the temperature.

Substituting the value of generalized strain according to Ref. [17] $e_{ii} = \frac{1}{n}\left[1 - (1 - 2e_{ii}^A)^{\frac{n}{2}}\right]$ in equation (6), we get:

$$\begin{aligned} T_{rr} &= \frac{E}{n(1-\nu)} - \frac{\beta^n E\{\nu + (1+P)^n\}}{n(1-\nu^2)} + \alpha\Theta, \\ T_{\theta\theta} &= \frac{E}{n(1-\nu)} - \frac{\beta^n E\{1 + \nu(1+P)^n\}}{n(1-\nu^2)} + \alpha\Theta, \\ T_{r\theta} &= T_{\theta z} = T_{zr} = T_{zz} = 0, \end{aligned} \tag{7}$$

where β varies radially and E Young's Modulus respectively. Radial equilibrium equation in cylindrical coordinates according to Ref. [19]:

$$\frac{d}{dr}(rT_{rr}) - T_{\theta\theta} + \rho\omega^2 r^2 = 0, \tag{8}$$

where ρ represents the density of the material of the rotating cylinder. Use (7) in (8), to obtain a non-linear differential equation in β as:

$$\begin{aligned} n\beta^{(n+1)}P(P+1)^{n-1}\frac{dP}{d\beta} =& r(1+\nu)\left(\frac{E'}{E} + \frac{\nu'}{1-\nu}\right) + \\ & \frac{nr(1-\nu^2)}{E}(\rho\omega^2 r + \alpha\Theta' + \alpha\Theta') + \\ & \beta^n\Big\{(1-\nu)\{1-(1+P)^n\} - \nu' r - \\ & \{\nu + (1+P)^n\}\Big\{\frac{2r\nu\nu'}{1-\nu^2} + \frac{E'r}{E} + np\Big\}\Big\}, \end{aligned} \tag{9}$$

where $r\beta' = \beta P$ ($P = f(\beta)$, and β depends on r).

3.4. Identification of the solution

To determine the transition stresses in a rotating disc, define the transition function(φ) according to Ref. [13–17, 20–31] at the critical point (transition point), that is at $P \to \pm\infty$,

$$\varphi = \frac{n}{2\mu}(T_{\theta\theta} - \alpha\Theta) = \frac{1+\nu}{1-\nu} - \frac{\beta^n\{1+\nu(1+P)^n\}}{1-\nu}. \tag{10}$$

After substituting the value of $\frac{dP}{d\beta}$ from (9) in (10) and considering $P \to \pm\infty$, we obtain:

$$\frac{d(log\varphi)}{dr} = -\frac{1-\nu}{r} - \frac{E'}{E} + \frac{\nu'}{(1+\nu)} + \frac{\nu'}{\nu}. \tag{11}$$

Now integrating the equation (11), we get:

$$\varphi = B_3\frac{\nu(1+\nu)}{rE}\exp\left(\frac{\nu_0 r^m}{ma^m}\right), \tag{12}$$

where B_3 are the constants of integration. which can be determined by boundary conditions, and Comparing the equation (12) and (10) to obtained the value of $T_{\theta\theta}$,

$$T_{\theta\theta} = \frac{B_3\nu\exp\left(\frac{\nu_0 r^m}{ma^m}\right)}{nr} + \alpha\Theta. \tag{13}$$

Substituting equation (13) in equation (8) using equations (1–5) and then integrating, we get:

$$T_{rr} = \frac{B_3}{nr}\exp\left(\frac{\nu_0 r^m}{ma^m}\right) + \frac{\alpha_0\Theta_0 r^{2m}}{a^{2m}(2m+1)} - \frac{\rho_0\omega^2 r^{2+m}}{a^m(3+m)} + \frac{B_4}{r}. \tag{14}$$

By using boundary condition $T_{rr} = 0 \quad at \quad r = a$, we obtain:

$$B_4 = \frac{\rho_0\omega^2 a^3}{3+m} - \frac{B_3\exp\left(\frac{\nu_0}{m}\right)}{n} - \frac{a\alpha_0\Theta_0}{2m+1}. \tag{15}$$

By using boundary condition $T_{rr} = f_{out} \quad at \quad r = b$,

$$B_4 = \frac{\rho_0\omega^2 b^{3+m}}{(3+m)a^m} - \frac{B_3\exp\left(\frac{\nu_0 b^m}{ma^m}\right)}{n} - \frac{\alpha_0\Theta_0 b^{2m+1}}{a^{2m}(2m+1)} + bf_{out}. \tag{16}$$

Now equating both equations (15 and 16), we obtained:

$$B_3 = \frac{n\rho_0\omega^2(a^{3+m} - b^{3+m}) - na^m b(3+m)f_{out}}{a^m(3+m)\left[\exp\left(\frac{\nu_0}{m}\right) - \exp\left(\frac{\nu_0 b^m}{ma^m}\right)\right]} - \frac{n\alpha_0\Theta_0(a^{2m+1} - b^{2m+1})}{a^{2m}(2m+1)\left[\exp\left(\frac{\nu_0}{m}\right) - \exp\left(\frac{\nu_0 b^m}{ma^m}\right)\right]}. \tag{17}$$

Put the value of B_3 in equation (15), we obtain B_4:

$$B_4 = \frac{\rho_0\omega^2 a^3}{3+m} - \frac{\rho_0\omega^2(a^{3+m} - b^{3+m}) - a^m b(3+m)f_{out}}{a^m(3+m)\left[\exp\left(\frac{\nu_0}{m}\right) - \exp\left(\frac{\nu_0 b^m}{ma^m}\right)\right]}\exp\left(\frac{\nu_0}{m}\right) + \frac{\alpha_0\Theta_0}{a^{2m}(2m+1)}\left[\frac{a^{2m+1}\exp\left(\frac{\nu_0 b^m}{ma^m}\right) - b^{2m+1}\exp\left(\frac{\nu_0}{m}\right)}{\exp\left(\frac{\nu_0}{m}\right) - \exp\left(\frac{\nu_0 b^m}{ma^m}\right)}\right]. \tag{18}$$

Now use the value of B_3, B_4 from equations (17,18) in equations (13 and 14),

$$T_{\theta\theta} = \frac{\rho_0\omega^2(a^{3+m} - b^{3+m}) - a^m b(3+m)f_{out}}{ra^m(3+m)\left[\exp\left(\frac{\nu_0}{m}\right) - \exp\left(\frac{\nu_0 b^m}{ma^m}\right)\right]}.\nu\exp\left(\frac{\nu_0 r^m}{ma^m}\right) + \frac{\alpha_0\Theta_0}{ra^{2m}}\left[r^{2m+1} - \frac{\nu(a^{2m+1} - b^{2m+1})\exp\left(\frac{\nu_0 r^m}{ma^m}\right)}{(2m+1)\left[\exp\left(\frac{\nu_0}{m}\right) - \exp\left(\frac{\nu_0 b^m}{ma^m}\right)\right]}\right]. \tag{19}$$

$$T_{rr} = \left\{\begin{array}{l} \frac{\rho_0\omega^2(a^{3+m} - b^{3+m}) - a^m b(3+m)f_{out}}{ra^m(3+m)\left[\exp\left(\frac{\nu_0}{m}\right) - \exp\left(\frac{\nu_0 b^m}{ma^m}\right)\right]}\exp\left(\frac{\nu_0 r^m}{ma^m}\right) - \\ \frac{\rho_0\omega^2(a^{3+m} - b^{3+m}) - a^m b(3+m)f_{out}}{ra^m(3+m)\left[\exp\left(\frac{\nu_0}{m}\right) - \exp\left(\frac{\nu_0 b^m}{ma^m}\right)\right]}\exp\left(\frac{\nu_0}{m}\right) - \\ \frac{\rho_0\omega^2(r^{3+m} - a^{3+m})}{ra^m(3+m)} + \frac{\alpha_0\Theta_0}{ra^{2m}(2m+1)}\left[r^{2m+1} + \right. \\ \frac{a^{2m+1}\left\{\exp\left(\frac{\nu_0 b^m}{ma^m}\right) - \exp\left(\frac{\nu_0 r^m}{ma^m}\right)\right\}}{\left[\exp\frac{\nu_0}{m} - \exp\frac{\nu_0 b^m}{ma^m}\right]} + \\ \left.\frac{b^{2m+1}\left\{\exp\left(\frac{\nu_0 r^m}{ma^m}\right) - \exp\left(\frac{\nu_0}{m}\right)\right\}}{\left[\exp\frac{\nu_0}{m} - \exp\frac{\nu_0 b^m}{ma^m}\right]}\right] \end{array}\right\}. \tag{20}$$

Now find the stress difference $|T_{rr} - T_{\theta\theta}|$ for elastic plastic deformation at $r = a$, $r = b$ from equations (19,20),

$$|T_{rr} - T_{\theta\theta}| = \left\{\begin{array}{l} \frac{\rho_0\omega^2(a^{3+m} - b^{3+m}) + a^m b(3+m)f_{out}}{ra^m(3+m)\left[\exp\left(\frac{\nu_0}{m}\right) - \exp\left(\frac{\nu_0 b^m}{ma^m}\right)\right]}\times \\ \left[(1-\nu)\exp\left(\frac{\nu_0 r^m}{ma^m}\right) - \exp\left(\frac{\nu_0}{m}\right)\right] - \\ \frac{\rho_0\omega^2(r^{3+m} - a^{3+m})}{ra^m(3+m)} + \frac{\alpha_0\Theta_0}{ra^m}\left[-\frac{2mr^{2m+1}}{2m+1} + \right. \\ a^{2m+1}\frac{\left\{\exp\left(\frac{\nu_0 b^m}{ma^m}\right) - (1-\nu)\exp\left(\frac{\nu_0 r^m}{ma^m}\right)\right\}}{(2m+1)\left[\exp\frac{\nu_0}{m} - \exp\frac{\nu_0 b^m}{ma^m}\right]} + \\ \left. b^{2m+1}\left\{\frac{(1-\nu)\exp\left(\frac{\nu_0 r^m}{ma^m}\right) - \exp\frac{\nu_0}{m}}{(2m+1)\left[\exp\frac{\nu_0}{m} - \exp\frac{\nu_0 b^m}{ma^m}\right]}\right\}\right] \end{array}\right\}. \tag{21}$$

$$|T_{rr} - T_{\theta\theta}|_{r=a} = \left\{\begin{array}{l} \frac{\rho_0\omega^2(a^{3+m} - b^{3+m}) + a^m b(3+m)f_{out}}{a^{m+1}(3+m)\left[\exp\left(\frac{\nu_0}{m}\right) - \exp\left(\frac{\nu_0 b^m}{ma^m}\right)\right]}\times \\ \left[-\nu\exp\left(\frac{\nu_0}{m}\right)\right] + \frac{\alpha_0\Theta_0}{a^{m+1}}\left[-\frac{2ma^{2m+1}}{2m+1} + \right. \\ a^{2m+1}\frac{\left\{\exp\left(\frac{\nu_0 b^m}{ma^m}\right) - (1-\nu)\exp\left(\frac{\nu_0}{m}\right)\right\}}{(2m+1)\left[\exp\frac{\nu_0}{m} - \exp\frac{\nu_0 b^m}{ma^m}\right]} - \\ \left. b^{2m+1}\left\{\frac{\nu\exp\left(\frac{\nu_0}{m}\right)}{(2m+1)\left[\exp\frac{\nu_0}{m} - \exp\frac{\nu_0 b^m}{ma^m}\right]}\right\}\right] \end{array}\right\} = Y(say). \tag{22}$$

For initial angular velocity,

$$\Omega_i^2 = \frac{\rho_0 \omega_i^2 b^2}{Y},$$

$$\Omega_i^2 = \left\{ \begin{array}{l} \dfrac{(3+m)a^{m+1}b^2\left[\exp\left(\frac{\nu_0}{m}\right) - \exp\left(\frac{\nu_0 b^m}{ma^m}\right)\right]}{(a^{3+m} - b^{3+m})\left[(1-\nu)\exp\left(\frac{\nu_0}{m}\right) - \exp\left(\frac{\nu_0 b^m}{ma^m}\right)\right]} - \\ \dfrac{a^m b^3 (3+m) f_{out}}{Y(a^{3+m} - b^{3+m})} - \\ \dfrac{\alpha_0 \Theta_0 (3+m) b^2 a^{2m+1}\left\{\exp\frac{\nu_0 b^m}{ma^m} - \exp\frac{\nu_0}{m}\right\}}{Y(a^{3+m} - b^{3+m})\left[(1-\nu)\exp\frac{\nu_0}{m} - \exp\frac{\nu_0 b^m}{ma^m}\right]} + \\ \dfrac{\alpha_0 \Theta_0 \nu (3+m) b^2 \exp\frac{\nu_0}{m}(a^{2m+1} - b^{2m+1})}{Y(2m+1)(a^{3+m} - b^{3+m})\left[(1-\nu)\exp\frac{\nu_0}{m} - \exp\frac{\nu_0 b^m}{ma^m}\right]} \end{array} \right\}. \quad (23)$$

The stress difference and angular velocity is higher at internal radii.

Obtaining all above relations in non-dimensional form:

$$\sigma_r = \frac{T_{rr}}{Y}, \sigma_\theta = \frac{T_{\theta\theta}}{Y}, \psi = \frac{r}{b}, \psi_0 = \frac{a}{b}, \Theta_1 = \frac{\alpha_0 \Theta_0}{Y(2m+1)}, F_{out} = \frac{f_{out}}{Y}$$

The stress obtained using equations (19,20,23) are following:

$$\sigma_r = \left\{ \begin{array}{l} \dfrac{\Omega_i^2(\psi_0^{3+m} - 1)(Z_1 - Z_3)}{\psi\psi_0^m(3+m)(Z_3 - Z_2)} - \\ \dfrac{F_{out}(Z_1 - Z_3)}{\psi(Z_3 - Z_2)} - \dfrac{\Omega_i^2(\psi^{3+m} - \psi_0^{3+m})}{\psi\psi_0(3+m)} + \\ \dfrac{\Theta_1(3+m)}{\psi\psi_0^{2m}}\left[\psi^{2m+1} + \dfrac{\psi_0^{2m+1}(Z_2 - Z_1)}{Z_3 - Z_2} + \dfrac{Z_1 - Z_3}{Z_3 - Z_2}\right] \end{array} \right\}, \quad (24)$$

$$\sigma_\theta = \left\{ \begin{array}{l} \dfrac{\Omega_i^2 \nu_0 \psi^{m-1}(\psi_0^{3+m} - 1)(Z_1)}{\psi_0^{2m}(3+m)(Z_3 - Z_2)} + \dfrac{F_{out}\nu_0\psi^{m-1}(Z_1)}{\psi_0^m(Z_3 - Z_2)} + \\ \dfrac{\Theta_1(2m+1)}{\psi\psi_0^{2m}}\left[\psi^{2m+1} + \nu_0 \dfrac{\psi^m(Z_1)(\psi_0^{2m+1} - 1)}{\psi_0^m(Z_3 - Z_2)(2m+1)}\right] \end{array} \right\}, \quad (25)$$

$$\Omega_i^2 = \left\{ \begin{array}{l} \dfrac{(3+m)\psi_0^{m+1}(Z_3 - Z_2)}{(\psi_0^{3+m} - 1)\left[(1-\nu)Z_3 - Z_2\right]} - \dfrac{\psi_0^m(3+m)F_{out}}{(\psi_0^{3+m} - 1)} - \\ \dfrac{\Theta_1(3+m)b^m\psi_0^{2m+1}\left\{(1+2m)Z_2 - (1+2m-\nu)Z_3\right\}}{(\psi_0^{3+m} - 1)\left[(1-\nu)Z_3 - Z_2\right]} + \\ \dfrac{\Theta_1(3+m)b^m\nu Z_3}{(\psi_0^{3+m} - 1)\left[(1-\nu)Z_3 - Z_2\right]} \end{array} \right\}, \quad (26)$$

where $Z_1 = \exp\left(\frac{\nu_0\psi^m}{m\psi_0^m}\right), Z_2 = \exp\left(\frac{\nu_0}{m\psi_0^m}\right), Z_3 = \exp\left(\frac{\nu_0}{m}\right)$.

4. Numerically illustration and discussion

Figures 1 and 2 show how radial stress, σ_r, changes with the ratio of radii (r/b) for various values of the non-homogeneity parameter m, Poisson's ratio ν, and a constant external load $F_{\text{out}} = -1$. The parameter m reflects how the material properties vary. Materials with $\nu < 0.5$ are compressible, while ν approaching 0.5 suggests an incompressible material.

In Figure 1, the radial stress exhibits a gradual decrease with increasing radii ratio and attains maximum compressive values near the outer boundary. At a lower Poisson's ratio ($\nu = 0.25$), the stress distribution is relatively smooth, while at higher Poisson's ratio ($\nu = 0.3$), stress accumulation becomes more prominent near the outer radius due to the restricted lateral deformation. The effect of the material parameter m is also significant: with increasing m, the stress gradients intensify, particularly in the boundary region, leading to higher compressive stresses. In Figure 2, the nature of the stress distribution changes considerably. The curve corresponding to $m = 3$ shows almost uniform compressive stress throughout the domain, while $m = 4$ produces the steepest decline in stress, resulting in maximum compressive values at the outer surface. Interestingly, at $m = 5$, the stress distribution becomes nearly flat, indicating a strong suppression of stress buildup even under the same external loading conditions. This behavior is attributed to the absence of volumetric deformation in incompressible media, which redistributes stresses more uniformly across the cylinder.

Figures 3 and 4 present the distribution of radial stress in the absence of external loading ($F_{out} = 0$) for compressible and incompressible materials, respectively. In the compressible cases ($\nu = 0.25, 0.3$), the stress decreases monotonically with the radii ratio, becoming more compressive toward the outer surface. At lower Poisson's ratio ($\nu = 0.25$), the stress variation is relatively smooth, whereas for higher Poisson's ratio ($\nu = 0.3$), stress accumulation near the boundary is more pronounced, indicating stronger constraint on lateral deformation. The influence of the material parameter m is particularly evident at $m = 5$, where $\nu = 0.25$ yields nearly negligible stress throughout the domain, while $\nu = 0.3$ results in substantial compressive stress at the boundary. For the incompressible case ($\nu = 0.5$), the stress magnitudes are comparatively higher across all m. The stress profile for $m = 3$ and $m = 4$ demonstrates a continuous decline with maximum compressive values near the outer surface, whereas for $m = 5$, the curve flattens, reflecting suppression of stress localization. These results establish that compressible materials are more sensitive to Poisson's ratio, while incompressible materials are governed primarily by the grading parameter m, which effectively controls the extent of stress uniformity.

Figures 5 and 6 show the radial stress response when an mechanical load is applied at the outer surface ($F_{out} = 1$) of the disc. In all cases the radial stress decreases monotonically with radii ratio and attains substantially larger compressive magnitudes at the outer boundary compared with the unloaded cases. For the compressible cases ($\nu = 0.25, 0.3$) In Fig. 5 the curves for $m = 3$ and $m = 4$ follow similar trends and reach large compressive values at $r/b \to 1$, whereas the influence of $m = 5$

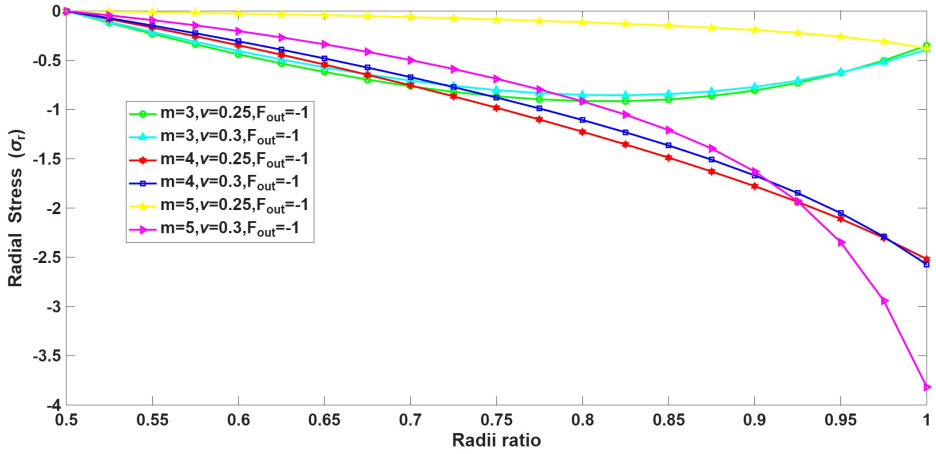

Figure 1. Radial stress at $F_{out} = -1$ for compressible material.

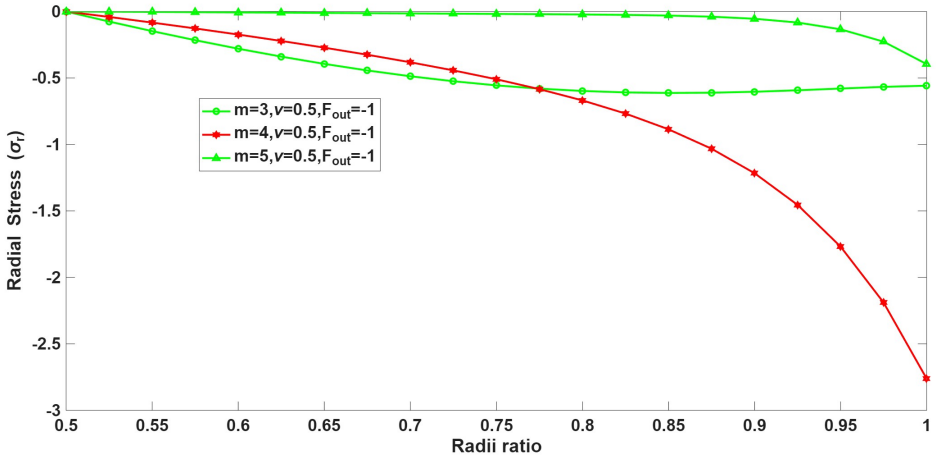

Figure 2. Radial stress at $F_{out} = -1$ for incompressible material.

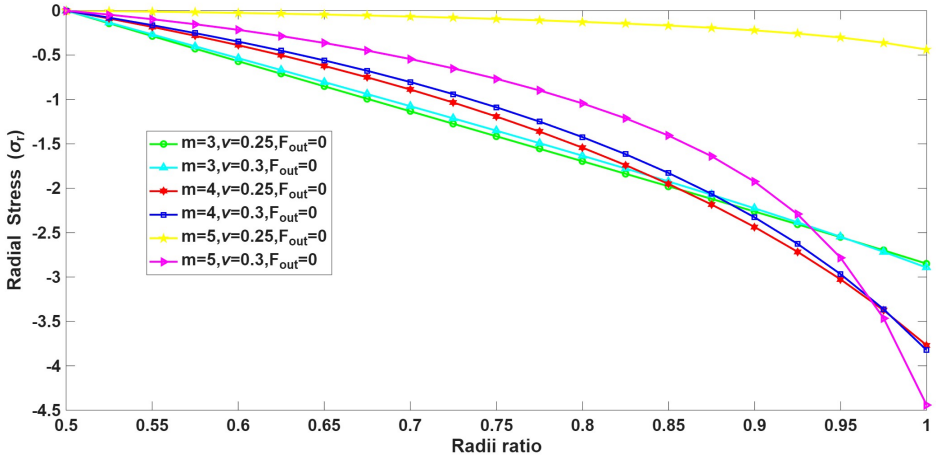

Figure 3. Radial stress at $F_{out} = 0$ for compressible material.

is strongly dependent on ν; as for $\nu = 0.25$ the $m = 5$ profile remains close to zero across most of the domain (i.e. stress buildup is effectively suppressed), but for $\nu = 0.3$ the $m = 5$ curve shifts toward much higher compression, producing some

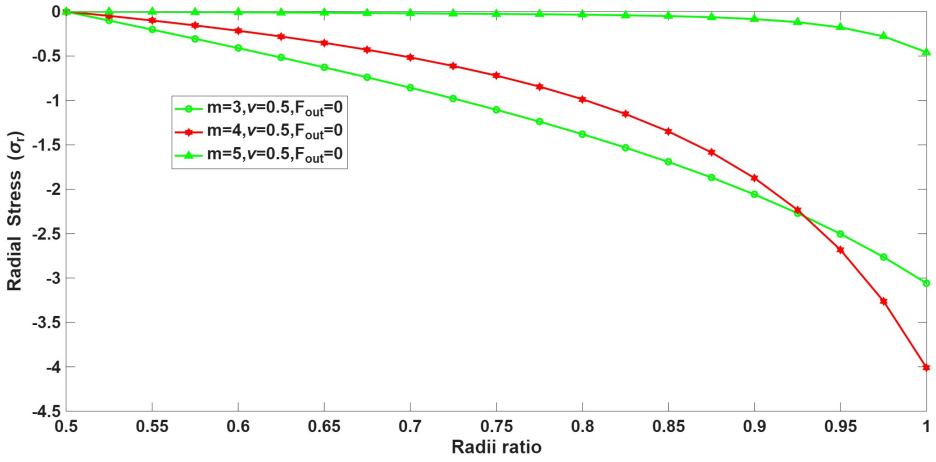

Figure 4. Radial stress at $F_{out} = 0$ for incompressible material.

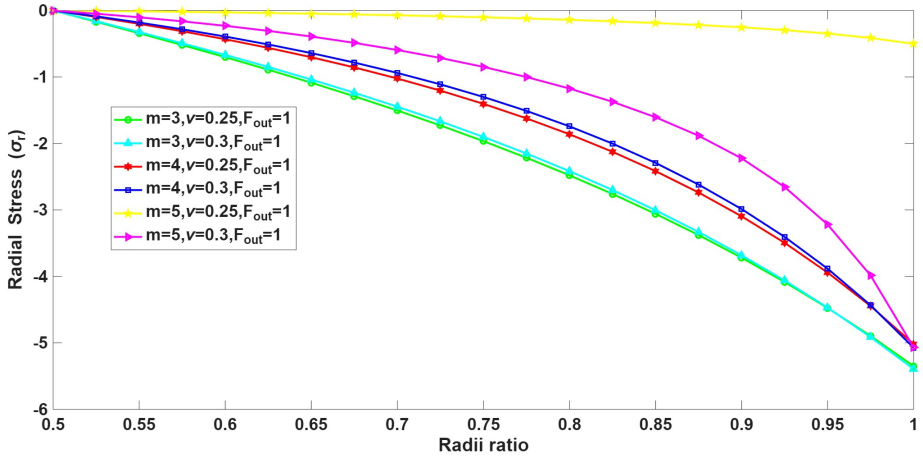

Figure 5. Radial stress at $F_{out} = 1$ for compressible material.

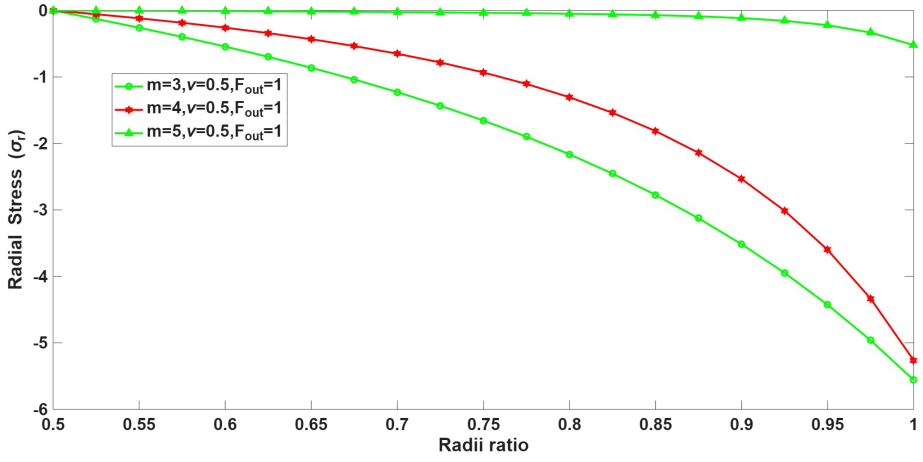

Figure 6. Radial stress at $F_{out} = 1$ for incompressible material.

of the largest negative σ_r values at the boundary. This indicates a coupled effect in which the same grading (large m) can amplify boundary stress depending on material compressibility.

For the incompressible case ($\nu = 0.5$) Fig. 6 the overall

compressive magnitudes are even larger; for $m = 3$ and $m = 4$ produce pronounced, progressively increasing compression toward the outer surface, while $m = 5$ again flattens the distribution and maintains very low compressive levels across the radius. Thus, in the incompressible limit the grading parameter m becomes the dominant control on stress localization – lower m concentrates stress at the boundary, and higher m (here $m = 5$) effectively suppresses that concentration. Thus, the application of an outward load increases radial compressive stress magnitudes overall, but by appropriate selection of m and ν one can either exacerbate or strongly reduce stress concentration at the outer surface – a useful design lever for tailoring the mechanical response of graded rotating cylinders.

In the absence of Internal load, the results are totally alinged with Ref. [23].

5. Conclusion

This study examined the stress response of a functionally graded rotating disc composed of compressible and incompressible materials under varying grading parameters (m), Poisson's ratios (ν), and external loading conditions. The results demonstrate that compressible materials ($\nu < 0.5$) exhibit higher stress magnitudes and sharper gradients, with radial stress (σ_r) showing stronger compression near the inner radius. The grading parameter m further amplifies these effects in compressible media, either intensifying or reducing boundary stress depending on the load direction. In contrast, incompressible materials ($\nu = 0.5$) reveal more uniform stress distributions with significantly reduced magnitudes, where the role of m becomes negligible. Outer surface loading ($F_{out} = 1$) produces the highest compressive stresses, while internal loading ($F_{out} = -1$) and unloaded cases ($F_{out} = 0$) highlight the interplay between material compressibility and gradation in governing stress localization. Overall, the findings suggest that incompressible-like FGMs are advantageous for minimizing boundary stress concentrations, enhancing durability, and reducing failure risks in high-performance rotating components such as aerospace rotors, pressure vessels, and advanced machinery. However, the study is limited by the assumptions of symmetric loading and purely elastic response, without considering thermal or dynamic effects, and by reliance on ideal gradation models, warranting experimental validation for broader practical applicability.

Data availability

No additional data was used beyond those presented in the submitted manuscript.

References

[1] M. Koizumi, "FGM activities in Japan", Composites Part B: Engineering **28** (1997) 1. https://doi.org/10.1016/S1359-8368(96)00016-9.

[2] D. K. Jha, T. Kant & R. K. Singh, "A critical review of recent research on functionally graded plates", Composite Structures **96** (2013) 833. https://doi.org/10.1016/j.compstruct.2012.09.001.

[3] Z. W. Wang, Q. Zhang, L. Z. Xia, J. T. Wu & P. Q. Liu, "Stress analysis and parameter optimization of an FGM pressure vessel subjected to thermo-mechanical loading", Procedia Engineering **130** (2015) 374. https://doi.org/10.1016/j.proeng.2015.12.230.

[4] A. B. Rad & M. Shariyat, "Thermo-magneto-elasticity analysis of variable thickness annular FGM plates with asymmetric shear and normal loads and non-uniform elastic foundations", Archives of Civil and Mechanical Engineering **16** (2016) 448. https://doi.org/10.1016/j.acme.2016.02.006.

[5] M. Adineh & M. Kadkhodayan, "Three-dimensional thermo-elastic analysis of multi-directional functionally graded rectangular plates on elastic foundation", Acta Mechanica **228** (2017) 881. https://doi.org/10.1007/s00707-016-1743-x.

[6] S. Habib, M. A. Hadek & A. Megharbel, "Stress analysis for cylinder made of FGM and subjected to thermo-mechanical loadings", Metals **9** (2018) 4. https://doi.org/10.3390/met9010004.

[7] Z. Li, J. Zheng, Q. Sun & H. He, "Nonlinear structural stability performance of pressurized thin-walled FGM arches under temperature variation field", International Journal of Non-Linear Mechanics **113** (2019) 86. https://doi.org/10.1016/j.ijnonlinmec.2019.03.016.

[8] A. Benslimane, R. Benchallal, S. Mammeri, M. Methia & M. A. Khadimallah, "Investigation of displacements and stresses in thick-walled FGM cylinder subjected to thermo-mechanical loadings", International Journal for Computational Methods in Engineering Science and Mechanics **22** (2020) 138. https://doi.org/10.1080/15502287.2020.1853853.

[9] E. Arslan, W. Mack & T. Apatay, "Thermo-mechanically loaded steel/aluminum functionally graded spherical containers and pressure vessels", International Journal of Pressure Vessels and Piping **191** (2021) 104334. https://doi.org/10.1016/j.ijpvp.2021.104334.

[10] R. Benchallal, A. Benslimane, O. Bidgoli & D. Hammiche, "Analytical solution for rotating cylindrical FGM vessel subjected to thermo-mechanical loadings", Materials Today: Proceedings **53** (2022) 24. https://doi.org/10.1016/j.matpr.2021.12.212.

[11] M. Lotfi, A. Loghman & M. Arefi, "Thermo-elastic analysis of functionally graded porous thick-walled cylindrical pressure vessels with variable thickness subjected to mechanical and thermal loading by higher order shear deformation theory", International Journal of Pressure Vessels and Piping **205** (2023) 105012. https://doi.org/10.1016/j.ijpvp.2023.105012.

[12] P. Das, A. Benslimane, M. A. Islam, A. A. Siddiquei & M. M. Rahman, "Finite element analysis of a generalized rotating vessel subjected to thermo-mechanical loadings: Effect of Poisson ratio and inhomogeneity parameters", Heliyon **10** (2024) e31833. https://doi.org/10.1016/j.heliyon.2024.e31833.

[13] P. Gulial & P. Thakur, "Exploring creep mechanisms in externally pressurised orthotropic cylinders with variable density", International Journal of Vehicle Design **96** (2024) 286. https://doi.org/10.1504/IJVD.2024.146776.

[14] A. Singh, P. Gulial & P. Thakur, "Exploring the effective stress behavior of internally pressurized cylinders with varying density", Journal of Applied Mathematics and Mechanics **104** (2024) e202400254. https://doi.org/10.1002/zamm.202400254.

[15] P. Thakur & P. Gulial, "Thermal and mechanical behavior of natural rubber and polystyrene disks under edge-loading: implications for structural integrity and thermal control", Journal of Rubber Research **28** (2025) 493. https://doi.org/10.1007/s42464-025-00316-3.

[16] B. R. Seth, "Transition theory of elastic-plastic deformation, creep and relaxation", Nature **195** (1962) 896. https://doi.org/10.1038/195896a0.

[17] B. R. Seth, "Measure concept in mechanics", International Journal of Non-Linear Mechanics **1** (1966) 35. https://doi.org/10.1016/0020-7462(66)90016-3.

[18] A. Benslimane, S. Bouzidi & M. Methia, "Displacements and stresses in pressurized thick-walled FGM cylinders: Exact and numerical solutions", International Journal of Pressure Vessels and Piping **168** (2018) 219. https://doi.org/10.1016/j.ijpvp.2018.10.019.

[19] H. Parkus, *Thermoelasticity*, Springer Science & Business Media, 2012.

[20] P. Thakur, "Elastic-plastic transition stresses in a thin rotating disc with rigid inclusion by infinitesimal deformation under steady-state temperature", Thermal Science **14** (2010) 209. https://doi.org/10.2298/TSCI1001209P.

[21] P. Thakur, "Deformation in a thin rotating disc having variable thickness and edge load with inclusion at the elastic-plastic transitional

stresses", Structural Integrity and Life, Serbia **12** (2012) 65. http://divk.inovacionicentar.rs/ivk/ivk12/065-IVK1-2012-TP.pdf.

[22] P. Thakur, J. Kaur & S. B. Singh, "Thermal creep transition stresses and strain rates in a circular disc with shaft having variable density", Engineering Computations **33** (2016). https://doi.org/10.1108/EC-05-2015-0110.

[23] N. Sharma, J. Kaur & P. Thakur, "Analysis of angular speed and stresses in a disc without mechanical load under varied temperature conditions", AIP Conference Proceedings **3231** (2024) 030004. https://doi.org/10.1063/5.0235869.

[24] P. Gulial & P. Thakur, "Influence of rotation and temperature on creep strain rates in steel and cast iron disks", ZAMM-Journal of Applied Mathematics and Mechanics **105** (2024) e202401253. https://doi.org/10.1002/zamm.202401253.

[25] P. Gulial & P. Thakur, "Investigating the effects of material density on strain rates in pressurized rotational cylinders", ZAMM-Journal of Applied Mathematics and Mechanics **105** (2025) e202401011. https://doi.org/10.1002/zamm.202401011.

[26] A. Sharma, J. Kaur & P. Thakur, "Study of transitional stresses in a rotating disk under the effect of different Poisson ratios", AIP Conference Proceedings **3231** (2024) 030007. https://doi.org/10.1063/5.0235966.

[27] A. Singh, P. Gulial & P. Thakur, "Exploring the effective stress behavior of internally pressurized cylinders with varying density", ZAMM-Journal of Applied Mathematics and Mechanics **104** (2024) e202400254. https://doi.org/10.1002/zamm.202400254.

[28] P. Gulial & P. Thakur, "Safety analysis in an elastoplastic orthotropic rotating cylinder under steady state temperature", Structural Integrity and Life **24** (2024) 309. https://doi.org/10.69644/ivk-2024-03-0309.

[29] P. Thakur, "Analytical solution of bending sheet made of cast iron/bronze material", Structural Integrity and Life **24** (2024) 305. https://doi.org/10.69644/ivk-2024-03-0305.

[30] P. Thakur, "Creep deformation in a thick-walled spherical shell having steady state temperature", Structural Integrity and Life **24** (2024) 301. https://doi.org/10.69644/ivk-2024-03-0301.

[31] S. Kumar, P. Thakur, S. Sood, N. Kumar & P. Gulial, "Transversely isotropic elastoplastic behaviour in a mechanically loaded rotating disk", Structural Integrity and Life **24** (2024) 167. https://doi.org/10.69644/ivk-2024-02-0167.

APPENDIX A.

Nomenclature

b	disc's external and
a	internal radii
u	Displacement in radial direction
w	Displacement in axial direction
v	Displacement in Tangential direction
β	$f(r)$, r is radius
r, z, θ	Radial, axial and circumferential direction
ω	Angular velocity of rotation
ρ	Density of material
E	Young's Modulus
T_{ij}	Stress tensor
B_1, B_2	Constants of integration
B_3, B_4	
Ω^2	angular velocity
σ_r	Radial stress component (T_{rr}/Y)
σ_θ	Circumferential stress component $(T_{\theta\theta}/Y)$
Θ	Temperature
δ_{ij}	Kronecker's delta function
α	Coefficient of thermal expansion
Θ_1	$(\frac{\alpha_0\Theta_0}{Y})$
ν	Poisson Ratio
m	non-homogeneity parameter
e_{ij}	strain component